NASA TECHNICAL NOTE

NASA TN D-3498

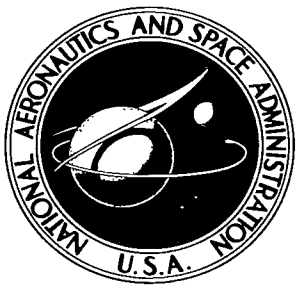

NASA TN D-3498

FLUTTER AT MACH 3 OF THERMALLY STRESSED PANELS AND COMPARISON WITH THEORY FOR PANELS WITH EDGE ROTATIONAL RESTRAINT

by John L. Shideler, Sidney C. Dixon, and Charles P. Shore

Langley Research Center
Langley Station, Hampton, Va.

NATIONAL AERONAUTICS AND SPACE ADMINISTRATION • WASHINGTON, D. C. • AUGUST 1966

FLUTTER AT MACH 3 OF THERMALLY STRESSED PANELS AND COMPARISON WITH THEORY FOR PANELS WITH EDGE ROTATIONAL RESTRAINT

By John L. Shideler, Sidney C. Dixon,
and Charles P. Shore

Langley Research Center
Langley Station, Hampton, Va.

NATIONAL AERONAUTICS AND SPACE ADMINISTRATION

For sale by the Clearinghouse for Federal Scientific and Technical Information
Springfield, Virginia 22151 – Price $1.00

FLUTTER AT MACH 3 OF THERMALLY STRESSED PANELS AND COMPARISON WITH THEORY FOR PANELS WITH EDGE ROTATIONAL RESTRAINT

By John L. Shideler, Sidney C. Dixon,
and Charles P. Shore
Langley Research Center

SUMMARY

An investigation was conducted at a Mach number of 3 in the Langley 9- by 6-foot thermal structures tunnel to study effects of thermal stress and buckling on the flutter characteristics of initially flat isotropic panels with length-width ratios of 2.5 and 2.9. The experimental results are presented in tabular form and are summarized graphically in terms of nondimensional flutter parameters. Comparison of experimental results with theory that accounts for edge rotational restraint showed good agreement at zero midplane stress and over a major portion of the flat panel flutter boundary. The theory was based on two-dimensional static aerodynamics. In the region of the transition from the flat panel boundary to the postbuckled boundary the agreement becomes poor. However, it is believed that accounting for panel initial imperfections in the theory may improve agreement between experiment and theoretical flutter boundaries in the transition region.

INTRODUCTION

The establishment of an adequate design criteria for the prevention of panel flutter has proved difficult because of the large number of parameters that affect the flutter characteristics of panels. One parameter that appears to be particularly significant is midplane compressive stress. The flutter of stressed panels has been the subject of a number of theoretical and experimental investigations. (See, for example, refs. 1 to 15.) These studies have indicated that considerable discrepancy may exist between theory and experiment. Theory predicts that the minimum dynamic pressure for flutter may occur at a value of midplane load less than that required for buckling. (See ref. 13.) However, existing experimental data show that the minimum value of dynamic pressure occurs at the transition from the boundary for flat unbuckled panels to the boundary for buckled panels. Most data on stressed panels have been obtained under aerodynamic heating conditions where thermal stresses have not been accurately known. Thus, the amount of disagreement between theory and experiment is uncertain.

In the present investigation, the effect of thermally induced stress on the flutter characteristics of flat rectangular panels is again considered with emphasis on those areas where discrepancies between theory and experiment exist. Tests were conducted at a Mach number of 3 in the Langley 9- by 6-foot thermal structures tunnel to obtain experimental data for panels with length-width ratios of 2.5 and 2.9. The experimental results presented in tabular form are summarized in terms of nondimensional flutter parameters and are compared with theory that accounts for panel edge rotational restraint. The theory is a closed-form solution which incorporates two-dimensional static aerodynamics. The average degree of rotational restraint was determined from the measured panel natural vibration frequencies.

SYMBOLS

The units used for the physical quantities defined in this paper are given both in the U.S. Customary Units and in the International System of Units, SI (ref. 16). The appendix presents factors relating these two systems of units.

a	panel length (longitudinal direction parallel to airflow)
B	width of frame and panel (see fig. 1)
b	panel width (lateral directional perpendicular to airflow)
c	constant (see eq. (1))
D	panel flexural stiffness, $\frac{Eh^3}{12(1 - \mu^2)}$
E	Young's modulus
f	flutter frequency
f_n	natural frequency of nth mode; $n = 1,2,3,4$
f_o	first natural frequency of a simply supported semi-infinite plate, $\frac{\pi}{2a^2}\sqrt{\frac{D}{\gamma h}}$
h	panel thickness
M	Mach number

N_x	inplane stress resultant in x-direction (positive in compression), $\sigma_x h$
N_y	inplane stress resultant in y-direction (positive in compression), $\sigma_y h$
ΔP	static differential pressure acting on panel skin (positive pressure deflects skin toward airstream)
q	free-stream dynamic pressure
q_x	rotational restraint coefficient on leading and trailing edges, $\frac{a\theta_x}{D}$
q_y	rotational restraint coefficient on side edges, $\frac{b\theta_y}{D}$
$\overline{R}_x$	nondimensional loading parameter, $\frac{N_x a^2}{\pi^2 D}$
T	panel skin temperature
T_t	free-stream stagnation temperature
ΔT	average increase of panel skin temperature
t	time
x	panel coordinate in direction parallel to airflow
y	panel coordinate in direction perpendicular to airflow
α	coefficient of thermal expansion of panel skin
$\beta = \sqrt{M^2 - 1}$	
γ	mass density of panel skin
θ_x, θ_y	rotational spring constants along the leading and trailing edges and along the side edges, respectively
μ	Poisson's ratio (taken equal to 0.3)
σ_x, σ_y	midplane stress in x- and y-direction, respectively (compression positive)

ψ modified temperature parameter, $\frac{12(1+\mu)}{\pi^2}\left\{\alpha\Delta T\left(\frac{a}{h}\right)^2 \pm c\left[\frac{|\Delta P|}{E}\left(\frac{a}{h}\right)^4\right]^{2/3}\right\}$

Subscripts:

n natural mode shape number (number of half-waves in x-direction)

T at transition point

EXPERIMENTAL INVESTIGATION

Panels

The panels consisted of flat sheets of 2024-T3 aluminum alloy of various thicknesses riveted to thick frames of the same material. The skin and frame were separated by a 0.031 inch (0.08 cm) strip of fiber glass insulation. In order to reduce initial stresses due to mounting, the frames were fastened to a mounting fixture (used to hold the panels during tests) before the sheets were riveted. For details of panel construction and mounting arrangement, see figures 1 to 4. The panels were 26 inches (66 cm) long and 10.4 and 9.0 inches (26.4 and 22.8 cm) wide (measured between the center lines of the rivets) corresponding to length-width ratios of 2.5 and 2.9, respectively.

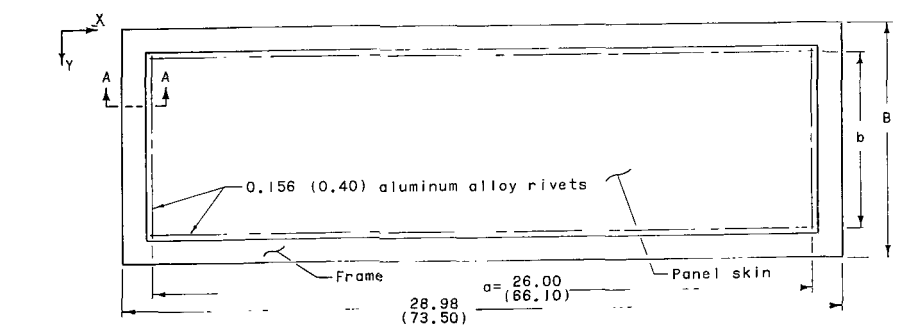

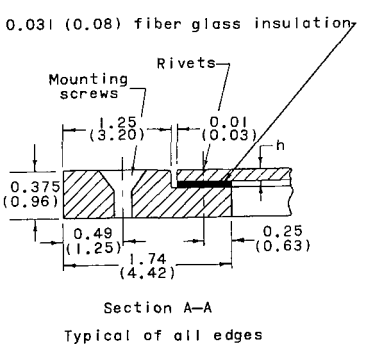

a/b	B	b	h
2.5	13.38 (34.0)	10.40 (26.4)	0.063 (0.16) 0.071 (0.18) 0.103 (0.26) 0.125 (0.32)
2.9	11.98 (30.4)	9.00 (22.8)	0.081 (0.21) 0.053 (0.13) 0.063 (0.16)

Table of dimensions

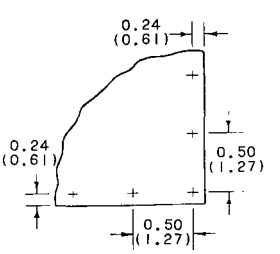

Rivet spacing

Figure 1.- Panel construction details (typical of all panels). All dimensions are in inches (cm).

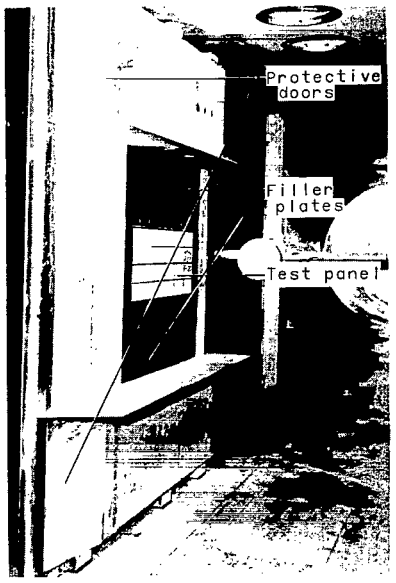

L-64-2337.1
Figure 2.- Panel holder in test section as viewed from upstream.

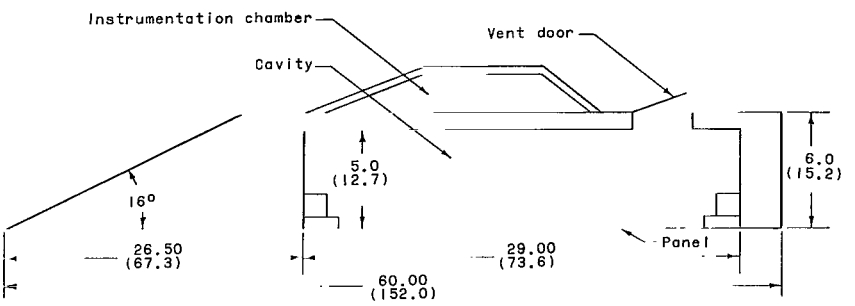

Figure 3.- Cross section of panel holder. All dimensions are in inches (cm).

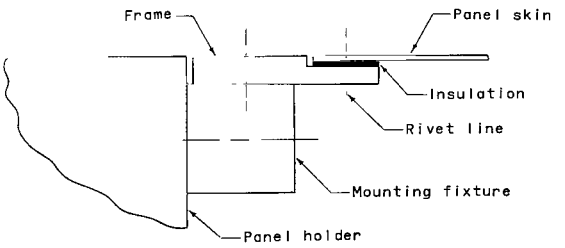

(a) Leading and trailing edge detail.

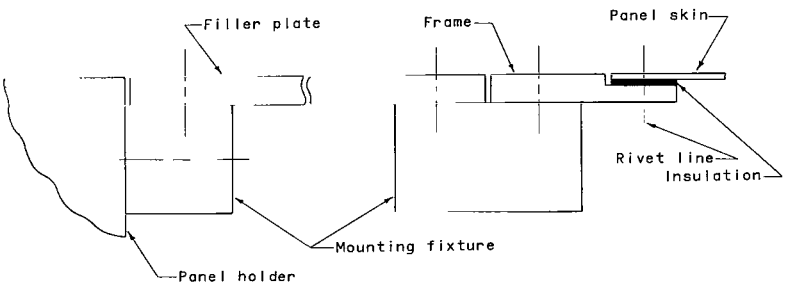

(b) Side edge detail.

Figure 4.- Panel mounting arrangement (typical of all panels).

Test Apparatus

Tunnel.- All tests were conducted in the Langley 9- by 6-foot thermal structures tunnel, a Mach 3 intermittent blowdown facility exhausting to the atmosphere. A heat exchanger is preheated to provide stagnation temperatures up to 660° F (622° K). The stagnation pressure can be varied from 60 to 200 psia (414 to 1379 kN/m^2 abs). Additional details on the tunnel are presented in reference 8.

Panel holder and mounting arrangement.- The panels were mounted in a panel holder which extended vertically through the test section (fig. 2). The panel holder has a beveled half-wedge leading edge with a recess on the nonbeveled side 29 inches (73.6 cm) wide, 30 inches (76 cm) high, and 5 inches (12.7 cm) deep for accommodating test specimens (fig. 3). Installation of instrumentation in the cavity and instrumentation chamber reduces the depth to approximately 3.5 inches (9 cm). Pneumatically operated sliding

doors protect test specimens from aerodynamic buffeting and heating during tunnel start and shutdown. Aerodynamic fences prevent shock waves emanating from the doors from interfering with the airflow over the test specimen. Results of pressure surveys indicate that the flow conditions over the exposed surface of a flat panel are essentially free-stream conditions (ref. 8). A vent door on the side opposite the recess is used to control the pressure inside the cavity behind the test specimen (fig. 3). To improve control of the differential pressure, all other openings to the cavity were sealed.

All panels were mounted flush with the flat surface of the panel holder. The test panels and the filler plates were attached with screws to the mounting fixture which had been bolted to the panel holder. (See figs. 2 and 4.)

Instrumentation

Iron-constantan thermocouples spotwelded to the back of the panel skins at 19 locations (see fig. 5) were used to measure panel temperatures. Variable-reluctance-type deflectometers were used to detect motion of the panel skin and to measure flutter frequencies. The deflectometers were located in the cavity approximately 1/4 inch (3/5 cm) behind the panel at the three positions indicated in figure 5. In addition, high-speed 16-mm motion pictures provided supplementary data on the behavior of the panels. Grid lines were painted on the panels for photographic purposes.

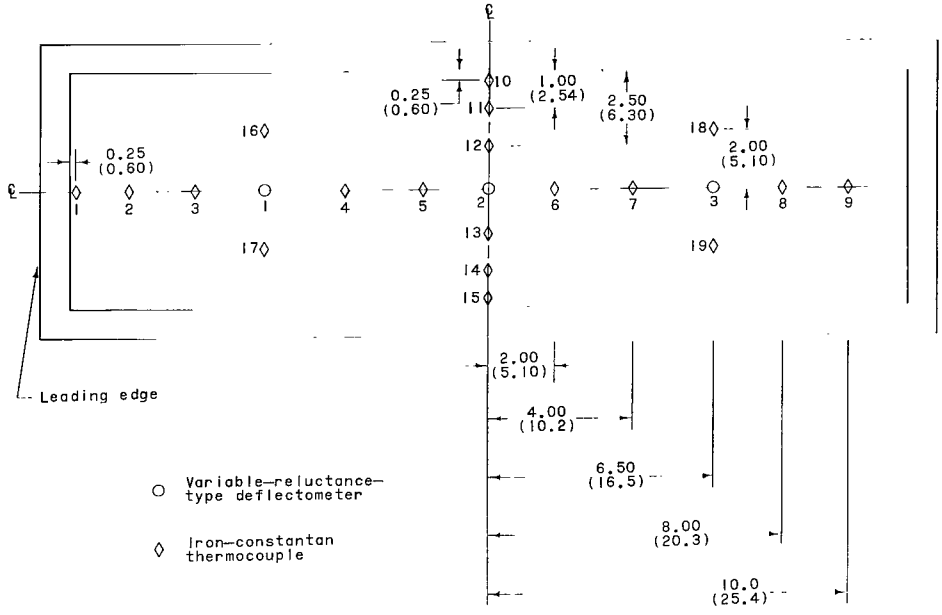

Figure 5.- Location of panel instrumentation (typical of all panels). All dimensions are in inches (cm).

Quick response strain-gage-type pressure transducers were used to measure static pressures at various locations on the panel holder and in the cavity behind the panel. Stagnation pressures in the test section were obtained from static pressure measurements in the tunnel settling chamber. Stagnation temperatures were measured by total temperature probes located in the test section. For each test, data from temperature and pressure transducers were recorded on magnetic tape every twentieth of a second. Deflectometer readings were recorded on a high-speed oscillograph.

Test Procedure

The panels were vibrated at sea-level conditions in the panel holder prior to each test with the air-jet shaker described in reference 17. Several panels attached to the mounting fixture were also vibrated prior to being installed in the panel holder so that the cavity behind the panels was essentially infinite. Comparison of the results indicated little effect on the natural vibration frequencies due to the change in cavity depth. The natural frequencies measured in the panel holder prior to each test are presented in table I. Also included are the theoretical natural frequencies for clamped and simply supported panels calculated from reference 18. Generally, the panel frequencies fell between the theoretical results for clamped and simply supported panels, and most frequencies were within 10 percent of the value for a clamped panel. No panel was tested if its frequencies differed from the theoretical value for a clamped panel by more than 25 percent. The mode shapes associated with the four frequencies f_n recorded during the vibration tests consisted of one half-wave in the cross-stream direction and n half-waves in the streamwise direction.

The wind-tunnel tests were conducted at a Mach number of 3, at dynamic pressures from 1500 to 5000 psf $(72$ to 240 $kN/m^2)$, and at stagnation temperatures from 300° F to 500° F (420° K to 530° K). The protective doors on the panel holder were opened after the desired test conditions were established and were closed 3 seconds prior to tunnel shutdown. The duration of test conditions varied from approximately 10 to 40 seconds. The stagnation temperature was essentially constant during each test. The differential pressure ΔP was maintained as near zero as possible by using a manual control. The dynamic pressure was constant during the first few seconds of each test, and only thermal stresses due to aerodynamic heating varied. However, during the latter part of several tests the dynamic pressure was varied in an attempt to obtain as many flutter points as possible. The occurrence of flutter was readily determined by monitoring the deflectometer traces on the high-speed oscillograph during the tests. The usual procedure for varying the dynamic pressure was as follows:

(a) If no flutter had occurred after a predetermined period of time, either the test was ended or the dynamic pressure was increased in an attempt to initiate flutter.

(b) If flutter had started and stopped, the dynamic pressure was increased in an attempt to restart flutter.

(c) If the panel was still fluttering after a predetermined period of time, the dynamic pressure was decreased in an attempt to stop flutter.

RESULTS AND DISCUSSION

The results of the investigation are presented in tables II and III in terms of the panel and wind-tunnel conditions at the beginning and cessation of flutter. The data tabulated include the stagnation temperature T_t, dynamic pressure q, panel skin temperature increase ΔT, differential pressure ΔP, and flutter frequency f. Data from tests in which no flutter occurred are tabulated at the highest value of the skin temperature increase ΔT attained (these tests were made at a constant dynamic pressure).

Panel Temperatures

At the beginning of each test, the panel skin and supporting structure were essentially at the same temperature. After a panel was exposed to the airstream, the skin temperature increased in a manner similar to the typical panel temperature history shown in figure 6. The upper curve represents the average of thermocouples 2 to 9, 12, 13, and 16 to 19. Individual temperatures for these thermocouples were within 10° F (5° K) of the average value. The lower two curves, which represent the average of thermocouples 11 and 14, and 1, 10, and 15, indicate a temperature gradient near the panel edges. These gradients, which are attributed to heat conduction to the supporting structure, were not accounted for in analyzing the test data. The average increase in temperature of thermocouples 2 to 9, 12, 13, and 16 to 19 was used as the uniform panel skin temperature increase ΔT which is employed in subsequent calculations.

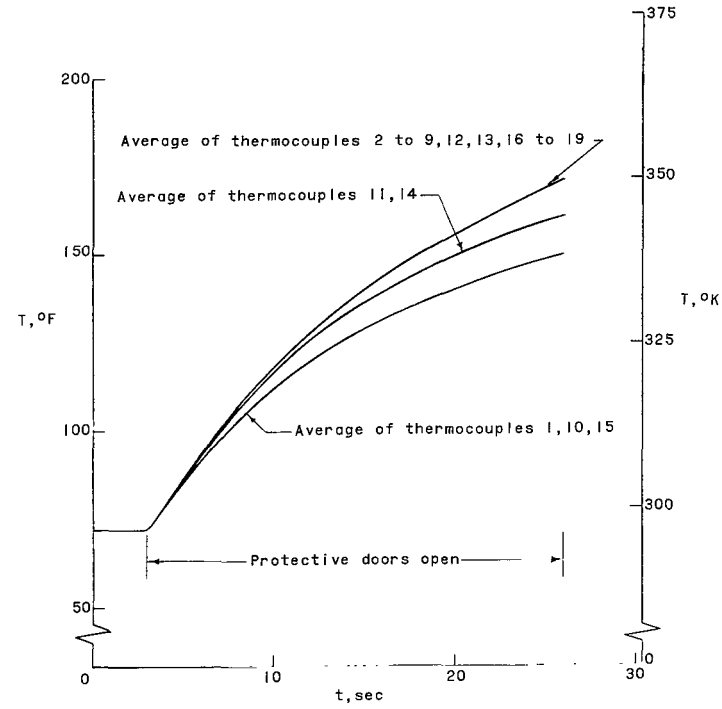

Figure 6.- Measured panel temperature history for test 12, typical of all tests. $\frac{a}{b} = 2.9$.

Flutter Parameters

The flutter data obtained in this investigation are summarized in terms of a dimensionless dynamic pressure flutter parameter and a dimensionless modified temperature parameter. Of the quantities in the flutter parameter $\left(\frac{q}{\beta E}\right)^{1/3}\frac{a}{h}$, which results from theoretical analyses employing two-dimensional static aerodynamics such as reference 1, only the dynamic pressure q and skin thickness h were varied in these tests. Because of the short duration of the tests and the relatively low panel temperatures, changes in material properties with temperature were assumed to be negligible.

Theoretical analyses indicate that the effect of midplane stress on the flutter parameter $\left(\frac{q}{\beta E}\right)^{1/3}\frac{a}{h}$ is a function of the loading parameter $\overline{R}_x$ where $\overline{R}_x = \frac{N_x a^2}{\pi^2 D}$. If N_x is assumed to be caused by complete restraint of thermal expansion on all edges corresponding to a uniform temperature increase ΔT, the loading parameter is equivalent to $\frac{12\alpha\Delta T(1+\mu)}{\pi^2}\left(\frac{a}{h}\right)^2$. Although thermal expansion was not completely restrained, this parameter is still useful as a measure of the actual thermal stress. Further, a differential pressure across the panel can also cause midplane stresses. This effect has been approximately accounted for in reference 9 by the addition of a pressure term to the temperature term to give

$$\psi = \frac{12(1+\mu)}{\pi^2}\left\{\alpha\Delta T\left(\frac{a}{h}\right)^2 \pm c\left[\frac{|\Delta P|}{E}\left(\frac{a}{h}\right)^4\right]^{2/3}\right\} \tag{1}$$

This modified temperature parameter ψ represents a measure of the midplane loading parameter $\overline{R}_x$. In the pressure term the minus sign applies when a panel is flat because a differential pressure causes tension. However, when a panel is buckled, the plus sign applies because ψ is then a measure of buckle depth and both ΔT and ΔP tend to increase the depth of buckle. The constant c is a function of $\frac{a}{b}$ and is determined from the experimental data by the method presented in reference 9. The empirical values obtained were 0.60 and 0.28 for the 2.5 and 2.9 length-width ratio panels, respectively. It should be emphasized that this differential pressure correction is only an approximation and becomes less accurate as the absolute value of ΔP increases.

Experimental Flutter Results

Flutter boundaries.- The flutter boundaries are shown in figure 7 $\left(\frac{a}{b} = 2.5\right)$ and figure 8 $\left(\frac{a}{h} = 2.9\right)$ in terms of the flutter parameter $\left(\frac{q}{\beta E}\right)^{1/3}\frac{a}{h}$ and the modified temperature parameter ψ. The open symbols represent flutter-start points (panel flat), whereas the open symbols with flags denote that the panel was buckled when flutter started. The

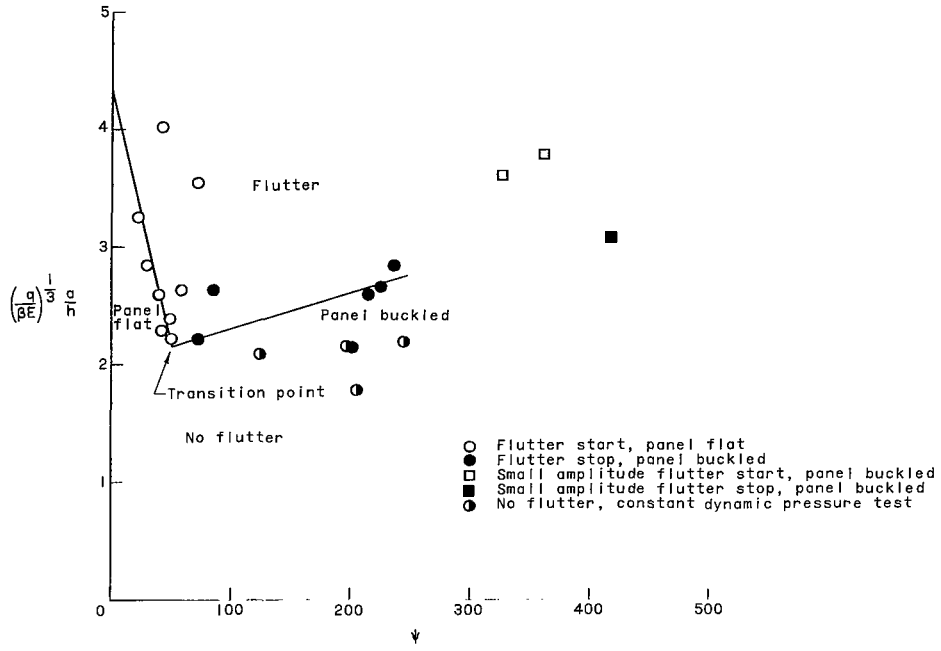

Figure 7.- Variation of flutter parameter with thermal stress. $\frac{a}{b} = 2.5$.

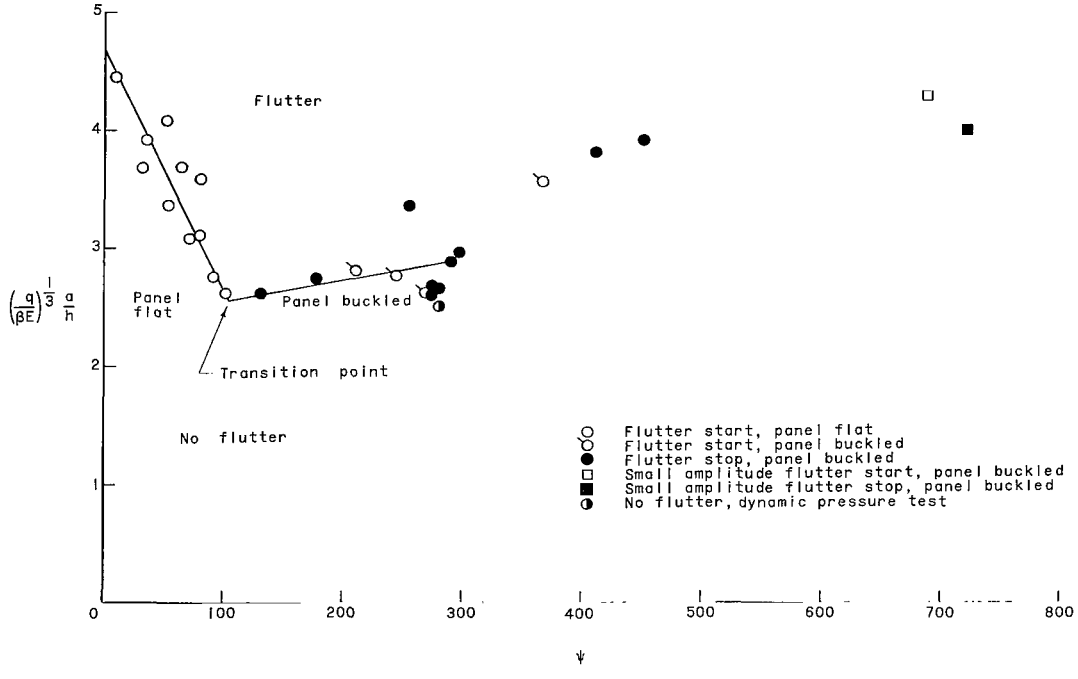

Figure 8.- Variation of flutter parameter with thermal stress. $\frac{a}{b} = 2.9$.

flutter-stop points (panel buckled) are represented by the solid symbols. The half-solid symbols denote the maximum value of ψ attained during tests in which no flutter occurred. These tests were made at a constant dynamic pressure, as previously noted. The curves shown are boundaries which have been faired through the experimental points. Each boundary consists of a flat panel portion and a buckled panel portion which intersect at a transition point, the minimum point of each boundary. For the panels with length-width ratio of 2.5 (fig. 7), the value of $\left(\frac{q}{\beta E}\right)^{1/3}\frac{a}{h}$ at the transition point (2.15) is 49 percent of its value at zero stress (4.35). Beyond the transition point, the boundary slopes upward. This behavior is attributed to the gradual increase of the stiffness as the buckle depth increases. For the panels with length-width ratio of 2.9 (fig. 8), the value of $\left(\frac{q}{\beta E}\right)^{1/3}\frac{a}{h}$ at the transition point (2.55) is 54 percent of its zero stress value (4.70). The "panel buckled" portion of the boundary slopes upward as did the boundary for $\frac{a}{b} = 2.5$. The general trend of each boundary is similar to previous experimental results. (See, for example, refs. 9 and 12.)

The square symbols at large values of ψ in figures 7 and 8 correspond to flutter-start and flutter-stop points of small amplitude motion about a buckled shape. This type of flutter will be discussed in the next section.

Flutter behavior.- The flutter observed from high-speed motion pictures appeared to be of the traveling wave type. However, in several tests, the motion during the first few seconds of flutter appeared to be more characteristic of the standing wave type. Predominantly standing wave flutter has been observed for panels with length-width ratios of 2 or less (refs. 9 and 12), whereas panels with length-width ratios of 4 or more have appeared to flutter in a traveling wave (refs. 7, 8, and 10). It follows that panels with length-width ratios between 2 and 4 could flutter in either a standing wave or a traveling wave or, perhaps, both. The flutter mode shape appeared to have two half-waves in the stream direction and one half-wave in the cross-stream direction as did the buckled mode shape at all flutter-stop points. This similarity between the flutter mode and buckling mode has been observed previously (refs. 7 and 8).

The flutter amplitude for panels with low stress was found to be at a maximum near the trailing edge as is indicated by both theory and experiment (refs. 2 and 10). For example, the amplitude and phase relation of the deflectometer records shown in figure 9(a) for test 4 $\left(\frac{a}{b} = 2.5\right)$ indicate that the maximum amplitude of motion lies near the center and between the center and rearward deflectometer locations. However, for panels with appreciable thermal stress when flutter started, the largest amplitude was found to be in the center as is indicated by the deflectometer traces shown in figure 9(b) for test 5 $\left(\frac{a}{b} = 2.5\right)$. As the panel stress approached the buckling stress, the maximum amplitude at

flutter start was observed to be nearer to the forward deflectometer than to the rearward deflectometer as indicated by the deflectometer amplitude and phase relation shown in figure 9(c) for test 8 $\left(\frac{a}{b} = 2.5\right)$. Theory indicates that the maximum amplitude can move upstream with an increase in stress (ref. 19). This phenomenon apparently has not been noted in previous experimental work and, generally, it was believed that no change in mode shape occurred as stress increased. (See ref. 13, for example.)

Motion pictures of the small amplitude flutter represented by square symbols in figures 7 and 8 revealed that the motion appeared as a standing wave superimposed on the buckle shape, with two half-waves perpendicular to the airflow. Because of its small amplitude, this flutter may not be damaging. However, scarcity of data prohibits any definite conclusions regarding the significance of this flutter.

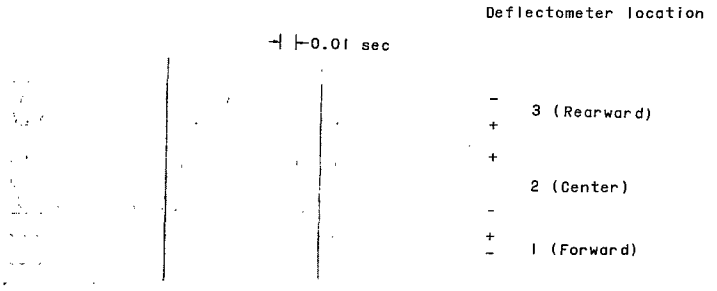

(a) Maximum amplitude rearward of center $\left(\text{test 4, } \frac{a}{b} = 2.5\right)$.

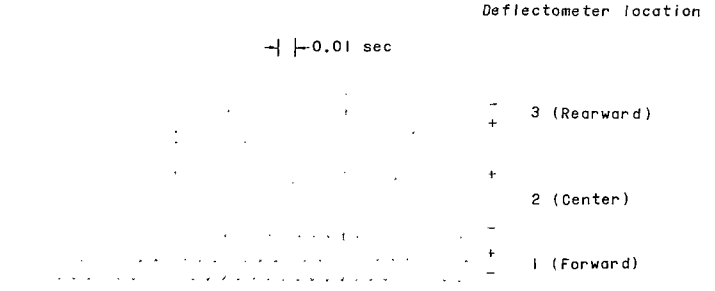

(b) Maximum amplitude near center $\left(\text{test 5, } \frac{a}{b} = 2.5\right)$.

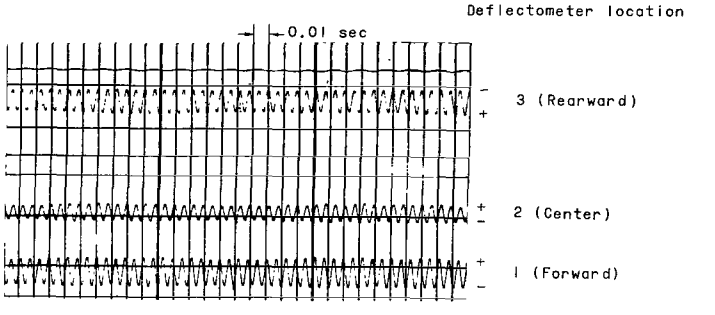

(c) Maximum amplitude forward of center $\left(\text{test 8, } \frac{a}{b} = 2.5\right)$.

Figure 9.- Sample deflectometer records (plus sign indicates outward panel deflection).

Analytical Results and Comparison With Experiment

As mentioned previously, the measured natural frequencies generally fell between the frequencies calculated for clamped edges and simply supported edges, indicating that the panel edge conditions were between those for clamped and simply supported. For this reason, experimental flutter results are compared with theoretical flutter results calculated from the closed-form solution of reference 1 for simply supported panels and with the approximate analysis of reference 2 for clamped panels. It should be noted that in reference 2 a cross-stream deflection function was assumed in order to reduce the

partial differential equation to an ordinary differential equation. The solution to the resulting ordinary differential equation, however, is exact. Clamped-beam modes from reference 20 were used as the cross-stream deflection function in the calculations for the clamped panel.

Calculations from these solutions, which use two-dimensional static aerodynamics, are compared with experimental data for $\frac{a}{b} = 2.5$ and $\frac{a}{b} = 2.9$ in figures 10 and 11, respectively. The dynamic pressure parameter is shown as a function of stress for simply supported and clamped panels with stress ratios of 1. The values of $\overline{R}_x$ at transition $\overline{R}_{x,T}$ were determined as those values of $\overline{R}_x$ at which the flutter frequency is zero. It should be noted that the curves in figures 10 and 11 are shown as functions of a stress ratio and not of stress itself. The value of $\overline{R}_{x,T}$ is smaller for the simply supported panel than for the clamped panel. Thus, at the same value of the abscissa, the stress in the panel is much higher if clamped edges are assumed rather than simply supported edges.

The "panel flat" portions of the experimental boundaries (from figs. 7 and 8) are included in figures 10 and 11 and are normalized by the value of the modified temperature parameter at the transition point ψ_T. For the condition of zero stress, figures 10 and 11 show that the experimental values of the flutter parameter are bracketed by the

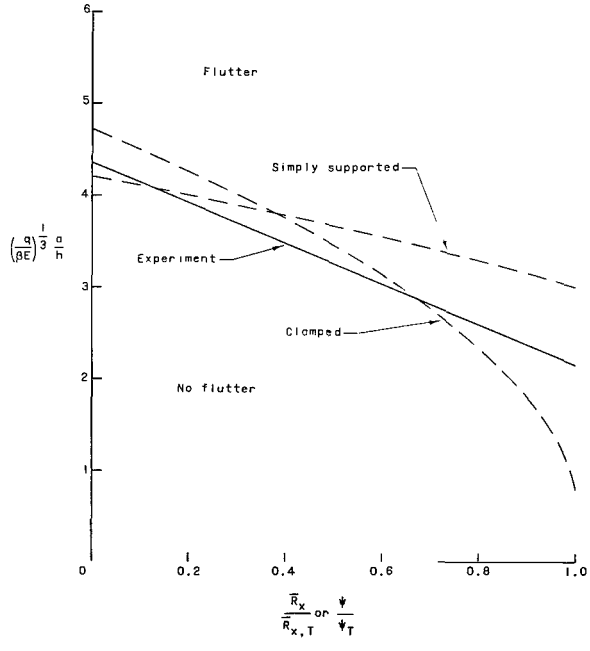

Figure 10.- Comparison of flat panel portion of faired experimental flutter boundary from figure 7 with theoretical boundary for panels with clamped and simply supported edges. $\frac{a}{b} = 2.5$; $\frac{N_y}{N_x} = 1.0$.

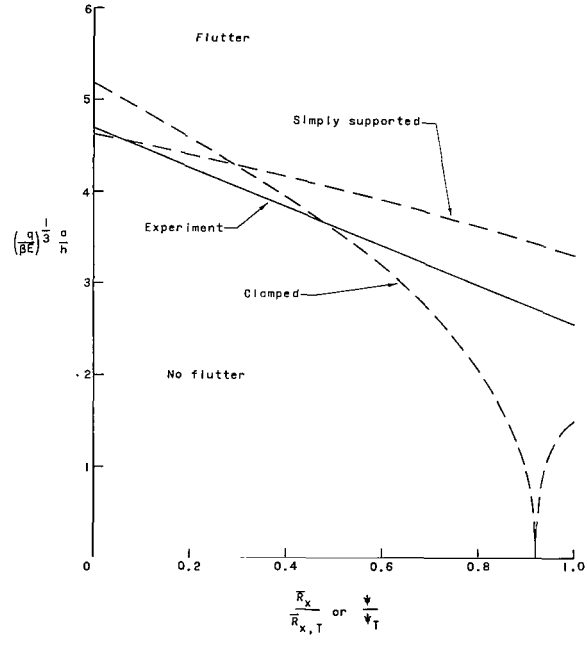

Figure 11.- Comparison of flat panel portion of faired experimental flutter boundary from figure 8 with theoretical boundary for panels with clamped and simply supported edges. $\frac{a}{b} = 2.9$; $\frac{N_y}{N_x} = 1.0$.

theoretical results for clamped and simply supported edges. Although agreement between theory and experiment is good at zero stress, it becomes poor as stresses approach buckling. For example, the theoretical clamped-panel flutter boundary for $\frac{a}{b} = 2.9$ (fig. 11) decreases to zero and then increases to the transition value. The theoretical results for clamped and simply supported panels presented in figures 10 and 11 suggest a large influence due to panel edge rotational restraint. Moreover, the measured natural frequencies, which were generally less than theory for panels with clamped edges, indicate that the experimental panels were neither clamped nor simply supported. The degree of rotational restraint which existed in the test panels was estimated for each test by using the results of reference 18, which gives panel natural vibration frequencies as a function of rotational restraint. The results of reference 18 are given in terms of nondimensional rotational restraint coefficients $q_x = \frac{a\theta_x}{D}$ and $q_y = \frac{b\theta_y}{D}$ where θ_x and θ_y are spring constants. Because of the uniformity of edge attachment it was assumed that the panels were supported with equal rotational restraint on all edges, that is, $\theta_x = \theta_y$. Thus, q_y is related to q_x by $q_y = \frac{b}{a} q_x$. The measured first natural frequencies of the test panels were used as inputs to calculate corresponding values of rotational restraint coefficient by using the numerical results from reference 18. From these values, average rotational restraint coefficients were determined to be $q_x = 85$ and $q_y = 34$ $\left(\text{for } \frac{a}{b} = 2.5\right)$ and $q_x = 44$ and $q_y = 15$ $\left(\text{for } \frac{a}{b} = 2.9\right)$. A few panels, those having the smallest thicknesses, had natural frequencies very near the theoretical values for clamped edges. (See, for example, tests 1 and 2, table I(a).) Flutter points for these panels usually fell above the faired experimental boundary. Since the boundary was established primarily on the basis of tests on panels with finite rotational restraint, the thinner panels that appeared to be essentially clamped (indicated by an asterisk in table I) were ignored in establishing the average rotational restraint.

The average of these rotational restraint coefficients and the theory of reference 19, which accounts for arbitrary degrees of rotational restraint, were used to calculate theoretical flutter boundaries. The theoretical transition points were again those values of $\overline{R}_x$ at which the flutter frequency is zero.

Experimental boundaries are compared with theoretical flutter boundaries in figure 12 $\left(\frac{a}{b} = 2.5\right)$ and in figure 13 $\left(\frac{a}{b} = 2.9\right)$ for panels having the calculated finite rotational restraint. These theoretical boundaries are in reasonable agreement with experiment not only at zero stress, but also over the major portion of the boundary. Only in the region of transition is the agreement poor. Comparison of figures 12 and 13 with figures 10 and 11, respectively, indicates that the inclusion of the effects of finite rotational restraint improves the agreement between theory and experiment. Thus, finite

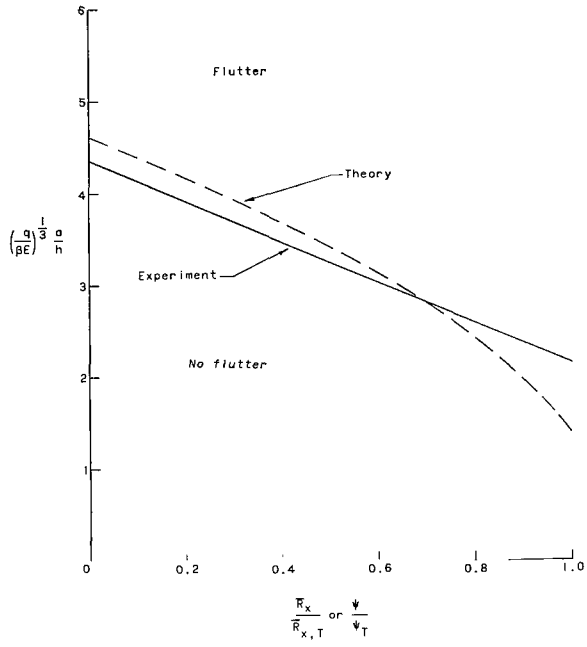

Figure 12.- Comparison of flat panel portion of faired experimental flutter boundary from figure 7 with theoretical boundary for panel with finite edge rotational restraint. $\frac{a}{b} = 2.5$; $\frac{N_y}{N_x} = 1.0$; $\theta_x = \theta_y$; $q_x = 85$.

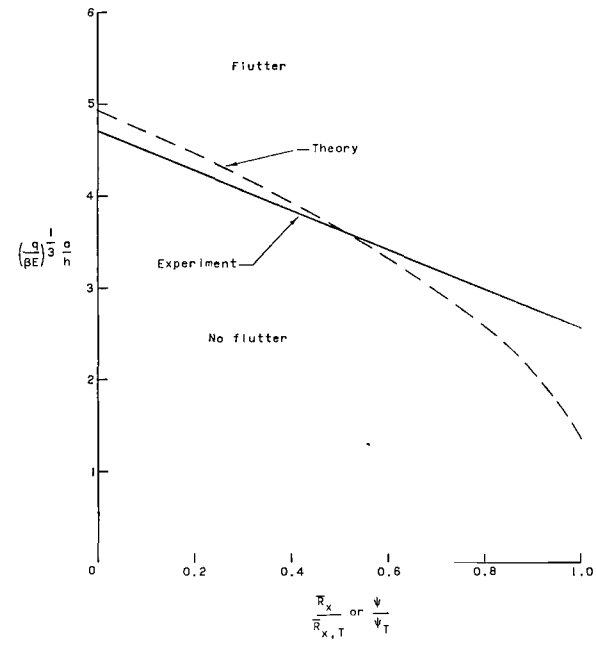

Figure 13.- Comparison of flat panel portion of faired experimental flutter boundary from figure 8 with theoretical boundary for panel with finite edge rotational restraint. $\frac{a}{b} = 2.9$; $\frac{N_y}{N_x} = 1.0$; $\theta_x = \theta_y$; $q_x = 44$.

rotational restraint has an important effect on the flutter behavior of a panel, especially in the region of high stress. (Note that the zero dynamic pressure flutter point indicated for the panel with clamped edges in figure 11 does not appear in figure 13.) Other factors such as length-width ratio and stress ratio also influence the flutter boundary, and more accurate definition of these factors may improve the agreement. Inclusion of aerodynamic and structural damping in the theoretical calculations can affect the results, but the effects of damping become small near the transition point where the greatest need for improvement exists.

Another factor, initial imperfections, can have an influence on the flutter behavior of stressed panels. For example, a two-mode analysis using two-dimensional quasi-steady aerodynamics (ref. 6) has shown that initial imperfections have a large effect on the flutter of compressively stressed semi-infinite panels. Thus, initial imperfections might also be the cause of the discrepancy between theory and experiment near the transition point for the panels of this investigation. Consideration of theoretical and experimental flutter frequencies also suggests the same cause. The variation of experimental flutter-start frequencies with stress is presented in figures 14 and 15 in terms of the dimensionless frequency ratio f/f_o and the dimensionless stress ratio ψ/ψ_T. Experimental frequencies in the buckled region are not shown. Theoretical flutter frequencies calculated from reference 19 for the two values of a/b are shown for comparison. At

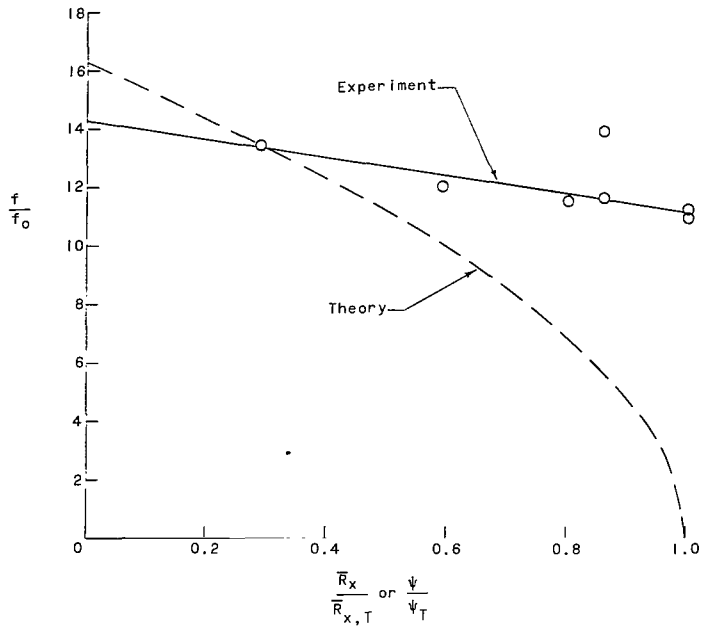

Figure 14.- Comparison of theoretical and experimental flutter frequencies. $\frac{a}{b} = 2.5$; $\frac{N_y}{N_x} = 1.0$; $\theta_x = \theta_y$; $q_x = 85$.

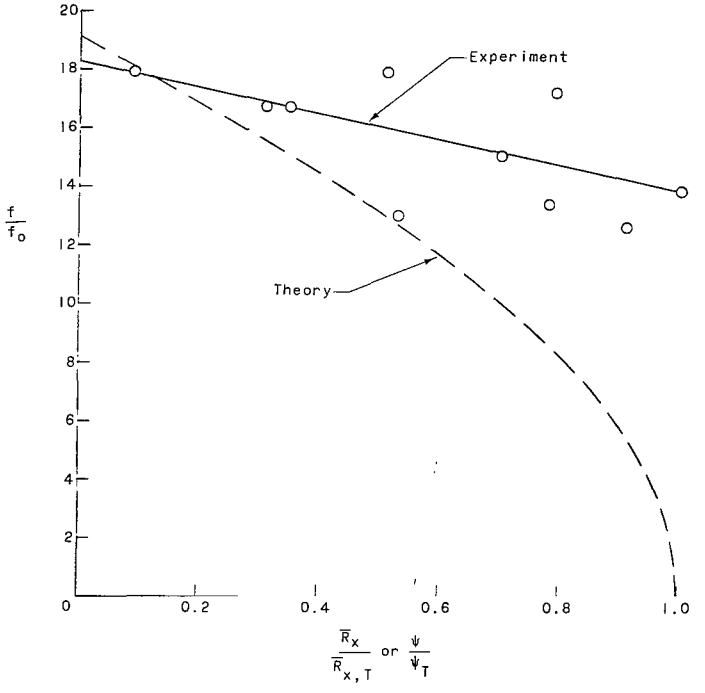

Figure 15.- Comparison of theoretical and experimental flutter frequencies. $\frac{a}{b} = 2.9$; $\frac{N_y}{N_x} = 1.0$; $\theta_x = \theta_y$; $q_x = 44$.

low stress the experimental flutter-start frequencies are in reasonable agreement with theory. At buckling, however, the theoretical flutter frequencies go to zero as is always true for a linear small deflection flutter analysis. The flutter-start frequencies did decrease as the stress at the flutter-start points increased, but these frequencies did not approach zero. The pronounced effect that initial imperfections have upon the natural vibration frequencies of stressed beams and plates is illustrated in references 21 and 22. Inclusion of initial imperfections in the analysis for stressed beams (ref. 21) eliminated the zero frequency values at buckling. The resulting theoretical natural frequencies agreed very well with measured frequencies. The effects of initial imperfections were also considered to contribute appreciably to the discrepancies between theoretical and experimental natural vibration frequencies for a plate near the region of buckling. Thus, the neglect of initial imperfections in the present panel flutter theory may be the cause of the discrepancy near transition.

CONCLUDING REMARKS

An investigation was conducted at a Mach number of 3 in the Langley 9- by 6-foot thermal structures tunnel to study the effects of thermal stress on the flutter characteristics of flat isotropic panels with length-width ratios of 2.5 and 2.9. The results revealed that the flutter boundaries consisted of a flat

panel portion, a buckled panel portion, and a transition point at their intersection. The boundaries are similar to experimental boundaries previously obtained for panels with length-width ratios from 0.96 to 10.

The flat panel flutter boundaries were compared with small deflection theory for simply supported and clamped edge conditions. Whereas agreement between theory and experiment was good at zero stress, it became poor as stresses approached buckling. By incorporating rotational restraint in theory, agreement between experimental and theoretical flutter boundaries was improved greatly; thus, the degree of edge rotational restraint has an important effect on panel flutter behavior. The faired experimental boundary was in reasonable agreement with theory for elastically restrained panels not only at zero stress but also over a major portion of the boundary. In the region of the transition point agreement remained poor.

Comparison of experimental flutter frequencies with theoretical flutter frequencies that account for rotational restraint revealed that for the condition of zero stress, the experimental frequencies were in good agreement with theory. However, for stresses that cause buckling, the experimental frequencies were considerably greater than the zero value predicted by the theory. It is believed that the inclusion of panel initial imperfections in the theory may improve the prediction of experimental and theoretical flutter frequencies for stressed panels and thereby improve agreement between experimental and theoretical flutter boundaries in the transition region.

Langley Research Center,
National Aeronautics and Space Administration,
Langley Station, Hampton, Va., December 9, 1965.

APPENDIX

CONVERSION OF U.S. CUSTOMARY UNITS TO SI UNITS

The International System of Units (SI) was adopted by the Eleventh General Conference on Weights and Measures, Paris, October 1960, in Resolution No. 12 (ref. 16). Conversion factors for the units used herein are given in the following table:

Physical quantity	U.S. Customary Unit	Conversion factor (*)	SI Unit
Length	in.	0.0254	meters (m)
Pressure	psf = lbf/ft^2	47.88	newtons per sq meter (N/m^2)
Stress	psi = lbf/in^2	6.895×10^3	newtons per sq meter (N/m^2)
Temperature	$(^oF + 459.67)$	5/9	degrees Kelvin (^oK)

*Multiply value given in U.S. Customary Unit by conversion factor to obtain equivalent value in SI Unit.

Prefixes to indicate multiple of units are as follows:

Prefix	Multiple
giga (G)	10^9
kilo (k)	10^3
centi (c)	10^{-2}
milli (m)	10^{-3}

REFERENCES

1. Hedgepeth, John M.: Flutter of Rectangular Simply Supported Panels at High Supersonic Speeds. J. Aeron. Sci., vol. 24, no. 8, Aug. 1957, pp. 563-573, 586.

2. Houbolt, John C.: A Study of Several Aerothermoelastic Problems of Aircraft Structures in High Speed Flight. Nr. 5, Mitteilungen aus dem Institut für Flugzeugstatik und Leichtbau, Leemann (Zürich), c.1958.

3. Fralich, Robert W.: Postbuckling Effects on the Flutter of Simply Supported Rectangular Panels at Supersonic Speeds. NASA TN D-1615, 1963.

4. Kobayashi, Shigeo: Flutter of Simply Supported Rectangular Panels in a Supersonic Flow. Trans. of Japan Soc. Aeron. and Space Sci., vol. 5, no. 8, 1962, pp. 79-89.

5. Kobayashi, Shigeo: Two-Dimensional Panel Flutter – I. Simply Supported Panel. Trans. of Japan Soc. Aeron. and Space Sci., vol. 5, no. 8, 1962, pp. 90-102.

6. Kobayashi, Shigeo: Two-Dimensional Panel Flutter – II. Clamped Panel. Trans. of Japan Soc. Aeron. and Space Sci., vol. 5, no. 8, 1962, pp. 103-118.

7. Dixon, Sidney C.: Application of Transtability Concept to Flutter of Finite Panels and Experimental Results. NASA TN D-1948, 1963.

8. Dixon, Sidney C.; Griffith, George E.; and Bohon, Herman L.: Experimental Investigation at Mach Number 3.0 of the Effects of Thermal Stress and Buckling on the Flutter of Four-Bay Aluminum Alloy Panels With Length-Width Ratios of 10. NASA TN D-921, 1961.

9. Dixon, Sidney C.: Experimental Investigation at Mach Number 3.0 of Effects of Thermal Stress and Buckling on Flutter Characteristics of Flat Single-Bay Panels of Length-Width Ratio 0.96. NASA TN D-1485, 1962.

10. Guy, Lawrence D.; and Bohon, Herman L.: Flutter of Aerodynamically Heated Aluminum-Alloy and Stainless-Steel Panels With Length-Width Ratio of 10 at Mach Number of 3.0. NASA TN D-1353, 1962.

11. Bohon, Herman L.: Panel Flutter Tests on Full-Scale X-15 Lower Vertical Stabilizer at Mach Number of 3.0. NASA TN D-1385, 1962.

12. Dixon, Sidney C.; and Shore, Charles P.: Effects of Differential Pressure, Thermal Stress, and Buckling on Flutter of Flat Panels With Length-Width Ratio of 2. NASA TN D-2047, 1963.

13. Guy, Lawrence D.; and Dixon, Sidney C.: A Critical Review of Experiment and Theory for Flutter of Aerodynamically Heated Panels. Symposium on Dynamics of Manned Lifting Planetary Entry, S. M. Scala, A. C. Harrison, and M. Rogers, eds., John Wiley & Sons, Inc., c.1963, pp. 568-595.

14. Bohon, Herman L.; and Dixon, Sidney C.: Some Recent Developments in Flutter of Flat Panels. J. Aircraft, vol. 1, no. 5, Sept.-Oct. 1964, pp. 280-288.

15. Bohon, Herman L.: Flutter of Flat Rectangular Orthotropic Panels With Biaxial Loading and Arbitrary Flow Direction. NASA TN D-1949, 1963.

16. Mechtly, E. A.: The International System of Units – Physical Constants and Conversion Factors. NASA SP-7012, 1964.

17. Herr, Robert W.; and Carden, Huey D.: Support Systems and Excitation Techniques for Dynamics Models of Space Vehicle Structures. Proceedings of Symposium on Aeroelastic and Dynamic Modeling Technology, RTD-TDR-63-4197, Pt. I, Aerospace Ind. Assoc., Mar. 1964, pp. 249-277.

18. Weeks, George E.; and Shideler, John L.: Effect of Edge Loadings on the Vibration of Rectangular Plates With Various Boundary Conditions. NASA TN D-2815, 1965.

19. Erickson, Larry L.: Effect of Boundary Conditions and Edge Loadings on the Flutter of Rectangular Panels. NASA TN D-3500, 1966.

20. Young, Dana; and Felgar, Robert P., Jr.: Tables of Characteristic Functions Representing Normal Modes of Vibration of a Beam. Publ. No. 4913, Eng. Res. Ser. No. 44, Bur. Eng. Res., Univ. of Texas, July 1, 1949.

21. Bisplinghoff, R. L.; and Pian, T. H. H.: On the Vibrations of Thermally Buckled Bars and Plates. Tech. Rept. 25-22, Office of Naval Res., Sept. 1956.

22. Lurie, Harold: Lateral Vibrations as Related to Structural Stability. J. Appl. Mech., vol. 19, no. 2, June 1952, pp. 195-204.

TABLE I.- NATURAL FREQUENCIES MEASURED PRIOR TO EACH TEST FOR TEST PANELS MOUNTED IN PANEL HOLDER

(a) $\frac{a}{b} = 2.5$.

		f_1, cps	f_2, cps	f_3, cps	f_4, cps	q_x
Panel 1	Clamped theory	131	154	194	258	∞
	Simply supported theory	63	90	133	194	0
	Test 1	[a]134	158	204	273	∞
	Test 2	[a]137	160	208	276	∞
Panel 2	Clamped theory	147	173	219	291	∞
	Simply supported theory	71	101	150	219	0
	Test 3	132	145	198	251	62.5
	Test 4	129	140	189	246	51.3
	Test 5	[a]149	166	227	300	∞
Panel 3	Clamped theory	214	251	317	422	∞
	Simply supported theory	103	146	218	317	0
	Test 6	[a]214	242	322	419	∞
	Test 7	201	225	295	393	108.0
	Test 8	203	233	307	407	129.0
	Test 9	198	231	311	415	87.0
	Test 10	197	227	309	412	85.2
Panel 4	Clamped theory	214	251	317	422	∞
	Simply supported theory	103	146	218	317	0
	Test 11	204	239	316	428	143.0
	Test 12	191	227	305	412	62.5
Panel 5	Clamped theory	259	304	384	512	∞
	Simply supported theory	125	177	264	384	0
	Test 13	217	250	339	462	40.0

(b) $\frac{a}{b} = 2.9$.

		f_1, cps	f_2, cps	f_3, cps	f_4, cps	q_x
Panel 1	Clamped theory	222	249	300	376	∞
	Simply supported theory	105	139	214	273	0
	Test 1	208	231	288	370	95.2
	Test 2	183	212	278	363	36.4
	Test 3	182	211	278	361	35.2
	Test 4	179	206	277	361	33.8
	Test 5	173	203	268	353	27.2
	Test 6	173	203	268	354	27.2
Panel 2	Clamped theory	145	163	196	247	∞
	Simply supported theory	69	91	140	179	0
	Test 7	[a]143	153	196	241	570.0
	Test 8	[a]141	102	201	---	222.0
	Test 9	[a]145	160	199	230	∞
Panel 3	Clamped theory	173	194	234	294	∞
	Simply supported theory	82	109	167	213	0
	Test 10	[a]173	190	245	313	∞
	Test 11	147	162	205	279	42.5
	Test 12	154	174	224	296	57.2
	Test 13	144	161	203	273	38.8

[a]Omitted in calculating average rotational restraint coefficient q_x.

TABLE II.- PANEL FLUTTER TEST DATA, $\frac{a}{b} = 2.5$

$\left[E = 10.5 \times 10^6 \text{ psi } \left(72.4 \text{ GN/m}^2\right);\ \alpha = 12.6 \times 10^{-6}\ {}^{o}\text{F}^{-1}\ \left(22.7 \times 10^{-6}\ {}^{o}\text{K}^{-1}\right)\right]$

Test	h		T_t		q		ΔT		ΔP		$\alpha \Delta T \left(\frac{a}{h}\right)^2$	$\left[\frac{\lvert\Delta P\rvert}{E}\left(\frac{a}{h}\right)^4\right]^{2/3}$	$\left(\frac{q}{\beta E}\right)^{1/3}\frac{a}{h}$	ψ	f, cps	Flutter start or stop	Panel condition (†)
	in.	mm	^{o}F	^{o}K	psf	kN/m^2	^{o}F	^{o}K	psi	kN/m^2							
1	0.063	1.60	310	428	2705	129.5	31	17.2	0.08	0.55	67	35	3.54	72	110	Start	F
2	.063	1.60	305	425	3910	187.2	17	9.4	.03	.21	37	18	4.01	42	125	Start	F
3	.071	1.80	305	425	2945	141.0	26	14.4	.26	1.8	44	59	3.25	22	135	Start	F
					1610	77.1	78	43.3	.04	.28	133	16	2.66	225	100	Stop	B
					4090	195.8	118	65.6	.08	.55	190	27	3.61	326	300	*Start	B
4	.071	1.80	300	422	1960	93.8	16	8.9	-.04	-.28	27	16	2.84	29	120	Start	F
					1950	93.4	82	45.6	.03	.21	141	13	2.84	236	100	Stop	B
5	.071	1.80	300	422	1480	70.9	29	16.1	.16	1.1	50	43	2.59	39	115	Start	F
					1480	70.9	75	41.7	.02	.14	129	11	2.59	214	105	Stop	B
					4650	222.6	126	70.0	.05	.34	217	18	3.79	360	290	*Start	B
					2505	119.9	152	84.4	.01	.07	261	4	3.08	417	310	*Stop	B
6	.103	2.62	305	425	3160	151.3	35	19.4	.01	.07	28	3	2.28	42	170	Start	F
7	.103	2.62	300	422	2445	117.1	89	49.4	.05	.34	74	7	2.09	123	---	No flutter	F-B
8	.103	2.62	350	450	2930	140.3	41	22.8	.01	.07	33	3	2.22	49	165	Start	F
					2920	139.8	54	30.0	.02	.14	43	4	2.22	72	155	Stop	B
9	.103	2.62	355	453	2670	127.8	152	84.4	.01	.07	123	3	2.16	197	---	No flutter	F-B
10	.103	2.62	355	453	4845	232.0	51	28.3	.05	.34	41	7	2.63	58	170	Start	F
					4830	231.3	61	33.9	.06	.41	49	8	2.63	85	160	Stop	B
11	.103	2.62	395	475	3640	174.3	42	23.3	.03	.21	33	5	2.39	49	160	Start	F
					2670	127.8	155	86.1	.03	.21	125	5	2.15	201	130	Stop	B
12	.103	2.62	485	525	1490	71.3	156	86.7	.02	.14	127	4	1.78	205	---	No flutter	F-B
13	.125	3.18	490	528	4920	235.6	280	155.6	.05	.34	152	4	2.19	244	---	No flutter	F-B

*Small amplitude.

†F denotes flat condition; B denotes buckled condition.

TABLE III.- PANEL FLUTTER TEST DATA, $\frac{a}{b} = 2.9$

$\left[E = 10.5 \times 10^6 \text{ psi } \left(72.4 \text{ GN/m}^2\right);\ \alpha = 12.6 \times 10^{-6}\ {}^\circ\text{F}^{-1}\ \left(22.7 \times 10^{-6}\ {}^\circ\text{K}^{-1}\right)\right]$

Test	h		T_t		q		ΔT		ΔP		$\alpha \Delta \dot{T} \left(\frac{a}{h}\right)^2$	$\left[\frac{\lvert\Delta P\rvert}{E}\left(\frac{a}{h}\right)^4\right]^{2/3}$	$\left(\frac{q}{\beta E}\right)^{1/3}\frac{a}{h}$	ψ	f, cps	Flutter start or stop	Panel condition (†)
	in.	mm	°F	°K	psf	kN/m²	°F	°K	psi	kN/m²							
1	0.081	2.06	350	450	4920	235.6	37	20.6	0.29	2.0	48	44	3.36	54	150	Start	F
					4865	232.9	121	67.2	.05	.34	158	14	3.35	255	95	Stop	B
2	.081	2.06	350	450	3905	187.0	43	23.9	.08	.55	56	19	3.11	80	155	Start	F
					2475	118.5	132	73.3	.11	.76	171	22	2.67	280	85	Stop	B
3	.081	2.06	375	464	2675	128.1	48	26.7	.05	.34	62	14	2.75	92	145	Start	F
					2675	128.1	84	46.7	.04	.28	109	12	2.74	177	130	Stop	B
					2890	138.4	101	56.1	.02	.14	131	6	2.82	210	100	Start	B
					2265	108.4	130	72.2	.05	.34	169	14	2.60	273	60	Stop	B
4	.081	2.06	350	450	2755	131.9	123	68.3	.08	.55	160	19	2.77	244	90	Start	B
					3350	160.4	136	75.6	.27	1.9	176	42	2.96	297	70	Stop	B
5	.081	2.06	350	450	1970	94.3	118	65.6	.14	.97	150	27	2.50	280	---	No flutter	F-B
6	.081	2.06	370	461	2335	111.8	54	30.0	.09	.62	70	20	2.62	102	160	Start	F
					2330	111.6	60	33.3	.08	.55	77	19	2.62	131	160	Stop	B
					2325	111.3	126	70.0	.10	.69	163	24	2.62	268	80	Start	B
					2500	119.7	130	72.2	.05	.34	169	14	2.68	274	90	Stop	B
7	.053	1.35	315	430	2455	117.5	17	9.4	.08	.55	52	58	4.08	52	135	Start	F
8	.053	1.35	300	422	1680	80.4	18	10.0	-.01	-.07	55	15	3.59	80	130	Start	F
9	.053	1.35	305	425	3190	152.7	16	8.9	.36	2.5	49	158	4.45	9	135	Start	F
10	.063	1.60	310	428	3055	146.3	25	13.9	.11	.76	53	44	3.68	64	(a)	Start	F
11	.063	1.60	300	422	3050	146.0	15	8.3	.10	.69	32	43	3.68	32	150	Start	F
12	.063	1.60	310	428	1710	81.9	23	12.8	-.03	-.21	50	18	3.08	72	135	Start	F
					1460	69.9	83	46.1	-.03	-.21	179	13	2.88	290	100	Stop	B
					2750	131.7	105	58.3	-.03	-.21	226	20	3.56	366	110	Start	B
					3410	163.3	114	63.3	.14	.97	244	54	3.82	410	110	Stop	B
13	.063	1.60	400	478	3675	176.0	17	9.4	.15	1.0	37	55	3.92	35	150	Start	F
					3655	175.0	130	72.2	.04	.28	279	21	3.92	450	105	Stop	B
					4765	228.1	203	112.7	.00	.00	435	0	4.28	687	270	*Start	B
					3895	186.5	211	117.2	.02	.14	452	13	4.00	720	270	*Stop	B

*Small amplitude.

†F denotes flat condition; B denotes buckled condition.

[a]Oscillograph did not operate.

"The aeronautical and space activities of the United States shall be conducted so as to contribute . . . to the expansion of human knowledge of phenomena in the atmosphere and space. The Administration shall provide for the widest practicable and appropriate dissemination of information concerning its activities and the results thereof."

—NATIONAL AERONAUTICS AND SPACE ACT OF 1958

NASA SCIENTIFIC AND TECHNICAL PUBLICATIONS

TECHNICAL REPORTS: Scientific and technical information considered important, complete, and a lasting contribution to existing knowledge.

TECHNICAL NOTES: Information less broad in scope but nevertheless of importance as a contribution to existing knowledge.

TECHNICAL MEMORANDUMS: Information receiving limited distribution because of preliminary data, security classification, or other reasons.

CONTRACTOR REPORTS: Technical information generated in connection with a NASA contract or grant and released under NASA auspices.

TECHNICAL TRANSLATIONS: Information published in a foreign language considered to merit NASA distribution in English.

TECHNICAL REPRINTS: Information derived from NASA activities and initially published in the form of journal articles.

SPECIAL PUBLICATIONS: Information derived from or of value to NASA activities but not necessarily reporting the results of individual NASA-programmed scientific efforts. Publications include conference proceedings, monographs, data compilations, handbooks, sourcebooks, and special bibliographies.

Details on the availability of these publications may be obtained from:

SCIENTIFIC AND TECHNICAL INFORMATION DIVISION

NATIONAL AERONAUTICS AND SPACE ADMINISTRATION

Washington, D.C. 20546